Quantifying covalency and metallicity in correlated compounds undergoing metal-insulator transitions

Ashish Chainani,[1,2] Ayako Yamamoto,[3] Masaharu Matsunami,[4] Ritsuko Eguchi,[4] Munetaka Taguchi,[4] Yasutaka Takata,[1] Hidenori Takagi,[3] Shik Shin,[4] Yoshinori Nishino,[1] Makina Yabashi,[1] Kenji Tamasaku,[1] and Tetsuya Ishikawa[1]

[1]*Coherent X-ray Optics Laboratory, RIKEN Harima Institute, 1-1-1 Sayo-cho, Hyogo 679-5148 Japan*

[2]*Department of Physics, Tohoku University, Aramaki, Aoba-ku, Sendai 980 8578 Japan*

[3]*RIKEN Advanced Science Institute, 2-1 Hirosawa, Wako, Saitama 351-0198 Japan*

[4]*Excitation-order Research Team, RIKEN Harima Institute, 1-1-1 Sayo-cho, Hyogo 679-5148 Japan*

(Received 28 October 2012; published 9 January 2013)

The tunability of bonding character in transition-metal compounds controls phase transitions and their fascinating properties such as high-temperature superconductivity, colossal magnetoresistance, spin-charge ordering, etc. However, separating out and quantifying the roles of covalency and metallicity derived from the same set of transition-metal d and ligand p electrons remains a fundamental challenge. In this study, we use bulk-sensitive photoelectron spectroscopy and configuration-interaction calculations for quantifying the covalency and metallicity in correlated compounds. The method is applied to study the first-order temperature-(T-) dependent metal-insulator transitions (MITs) in the cubic pyrochlore ruthenates $Tl_2Ru_2O_7$ and $Hg_2Ru_2O_7$. Core-level spectroscopy shows drastic T-dependent modifications which are well explained by including ligand-screening and metallic-screening channels. The core-level metallic-origin features get quenched upon gap formation in valence band spectra, while ionic and covalent components remain intact across the MIT. The results establish temperature-driven Mott-Hubbard MITs in three-dimensional ruthenates and reveal three energy scales: (a) 4d electronic changes occur on the largest (∼eV) energy scale, (b) the band-gap energies/charge gaps ($E_g \sim$ 160–200 meV) are intermediate, and (c) the lowest-energy scale corresponds to the transition temperature T_{MIT} (∼10 meV), which is also the spin gap energy of $Tl_2Ru_2O_7$ and the magnetic-ordering temperature of $Hg_2Ru_2O_7$. The method is general for doping- and T-induced transitions and is valid for V_2O_3, CrN, $La_{1-x}Sr_xMnO_3$, $La_{2-x}Sr_xCuO_4$, etc. The obtained transition-metal–ligand (d–p) bonding energies ($V \sim$ 45–90 kcal/mol) are consistent with thermochemical data, and with energies of typical heteronuclear covalent bonds such as C-H, C-O, C-N, etc. In contrast, the metallic-screening energies of correlated compounds form a weaker class ($V^* \sim$ 10–40 kcal/mol) but are still stronger than van der Waals and hydrogen bonding. The results identify and quantify the roles of covalency and metallicity in 3d and 4d correlated compounds undergoing metal-insulator transitions.

DOI: 10.1103/PhysRevB.87.045108 PACS number(s): 71.30.+h, 79.60.−i, 71.27.+a, 33.15.Fm

I. INTRODUCTION

The wide range of physical and chemical properties of transition-metal compounds (TMCs) arise from the versatile bonding behavior of metal d electrons combining with ligand p electrons.[1–11] Well-known examples include high-temperature copper-oxide superconductors and colossal magnetoresistance (CMR) manganese oxides, which are based on compounds of the A_2MO_4 and AMO_3 perovskite structure,[2,3] respectively (A: s,p-block/rare-earth element, M: transition metal, O: oxygen). These materials, as well as many low-dimensional binary and ternary oxides (such as bronzes: A_xMO_3, Magneli compounds: M_nO_{3n-1}, etc.) exhibit electronic instabilities[4] derived from charge and spin degrees of freedom of an octahedral MO_6 motif acting as the basic building block. Pyrochlore oxides of the general formula $A_2M_2O_7$ have also revealed novel properties[5–11] based on the octahedral MO_6 motif, often with the additional role of frustration effects inherent to its structure. Important realizations include metal-insulator transition[6] (MIT) in $Bi_{2-x}Y_xRu_2O_7$, giant magnetoresistance[8] (GMR) in $Tl_2Mn_2O_7$, spin ice[9] in $Dy_2Ti_2O_7$, MIT and orbital ordering of spin chains[10] in $Tl_2Ru_2O_7$, superconductivity[11] in $Cd_2Re_2O_7$, etc. While the importance of strong electron-electron correlations is well accepted for 3d TMCs, their role is often doubted for three-dimensional 4d and 5d TMCs due to the larger extent of the 4d and 5d orbitals.[12] This is in spite of the fact that a purely electronic Mott-Hubbard transition[13] and an orbital ordering transition[14] have been discovered in quasi-two-dimensional (quasi-2D) layered ruthenate compounds. The alternate picture for the pyrochlores is based on the A-site states (e.g., Bi 6s/Tl 6s) playing the dominant role for driving the spin-charge-lattice coupled properties such as MIT and GMR.[15–18] We resolve this issue by using bulk-sensitive photoelectron spectroscopy of ruthenate pyrochlores which exhibit first-order MITs as a function of temperature (T). Further, while the usage of the term "metallic bonding" has been debated in the literature to be a subset of covalent bonding,[19,20] we use the MIT in the ruthenates and a variety of TMCs to unambiguously show the qualitative and quantitative differences between covalent bonding of metal d with ligand p states compared to metallicity associated with the correlated d-electron states. Here, it is emphasized that we are addressing the metallicity or metallic screening in compounds which exhibit correlation effects in their electronic structure in the form of TM d character coherent and incoherent states. Such electronic structures are well known in many 3d TMCs and can be suitably described by dynamical mean-field theory (DMFT).[21,22] It is noted that we are not addressing the metallic bond of simple elemental metals or intermetallics, which can

be described by band-structure calculations in the absence of strong correlations.

In the context of a non-3*d* TMC, the recent discovery[23,24] of a MIT in $Hg_2Ru_2O_7$ has added an important aspect to properties of strongly correlated compounds. It was shown that $Hg_2Ru_2O_7$ exhibits a sharp transition at $T_{MIT} = 108$ K, with hysteresis in the electrical resistivity and magnetic susceptibility as a function of T. The high-T magnetic susceptibility showed that the effective magnetic moment was typical of a Ru^{5+} ion corresponding to a t_{2g}^3, $S = \frac{3}{2}$ configuration.[24] In comparison, the analogous MIT in $Tl_2Ru_2O_7$ showed an orbital ordering of Haldane spin chains with Ru^{4+} ions in a t_{2g}^4, $S = 1$ configuration.[10] This raises the following important question: Since the t_{2g}^3 configuration of $Hg_2Ru_2O_7$ can not accommodate orbital order, while $Tl_2Ru_2O_7$ is an orbitally ordered system, does the MIT result from changes in the Ru 4*d* electrons or from other electronic states?

More specifically, in terms of the Zaanen-Sawatzky-Allen classification,[25] do the pyrochlore ruthenates possess (i) a lowest-energy excitation of *d*-*d* character (Mott-Hubbard: MH type), i.e., the first ionization state and the lowest electron affinity state have Ru 4*d* character or (ii) is it of ligand *p* and metal *d* character (charge transfer: CT type) with the first ionization state of O 2*p* and the electron affinity state of Ru 4*d* type? Photoelectron spectroscopy studies played an important role in establishing this classification and typical examples of the two types are V_2O_3 (Refs. 26–28) and the high-T_c copper-oxide superconductors.[29,30] Figures 1(a) and 1(b) show schematic diagrams of the difference in their electronic structure, which mainly reflects the fact that in an isostructural series, the onsite *d*-*d* Coulomb repulsion energy (U_{dd}) increases systematically from early to late TMCs.[25] Consequently, $U_{dd} < \Delta$ describes MH compounds [Fig. 1(a)] with a *d*-*d* band gap, while $U_{dd} > \Delta$ characterizes CT compounds [Fig. 1(b)], where Δ is the charge-transfer energy determining the band gap, and is the energy separation between the ligand *p* and metal *d* states.

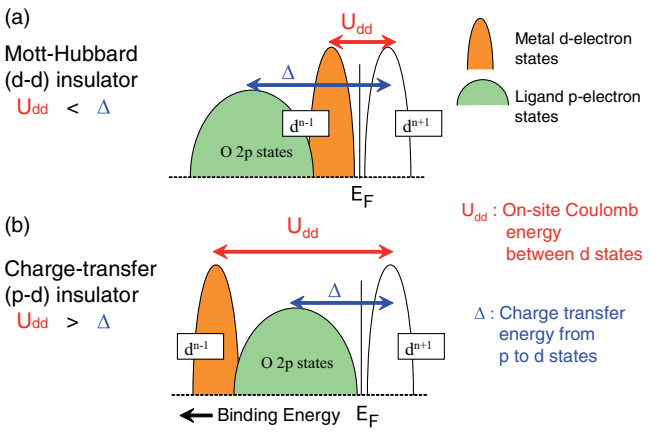

FIG. 1. (Color online) Schematics of the electronic structure of transition-metal compounds can be generally classified into (a) a *d*-*d* character Mott-Hubbard insulator and (b) a *d*-*p* character charge-transfer insulator. These insulating ground states give rise to the Mott-Hubbard metal or the charge-transfer metal, respectively, as a function of doping, temperature, or pressure.

Another important issue relates to the coupled behavior of the valence band and core-level states as investigated by photoelectron spectroscopy. An early study on composition-dependent but T-independent MITs in a series of pyrochlore ruthenates showed that the Ru 3*d* core-level photoelectron spectra exhibit well-screened and poorly screened states which change with composition.[6] A more recent study has systematized these changes using DMFT calculations of the MIT in a single-band approximation without orbital degeneracy.[31] The study showed that the core-level changes are coupled to the calculated changes in the valence band. The metallic phase is obtained by formation of coherent states at the Fermi level (E_F), as a result of spectral weight transfer from the MH bands of the insulator. While this is well accepted for 3*d* TMCs,[21,22] this interpretation has been recently challenged for the MIT in ruthenates.[32] On the basis of multisite cluster calculations,[32] it was predicted that a competition between local and nonlocal screening in the presence of orbital ordering can explain the Ru 3*d* core-level experimental spectra, without the need of invoking additional states at E_F. While an early soft x-ray electron spectroscopy study on $Tl_2Ru_2O_7$ showed changes in the valence and conduction band states, the Ru 3*d* core-level spectra were not reported.[17] This study reports the T-dependent valence band and core-level spectra of $Tl_2Ru_2O_7$ and $Hg_2Ru_2O_7$. $Tl_2Ru_2O_7$ and $Hg_2Ru_2O_7$ are appropriate examples of isostructural compounds showing T-dependent first-order MITs, with and without orbital order, respectively. We use synchrotron-based hard x-ray ($h\nu \sim 8$ keV) electron spectroscopy for chemical analysis (ESCA), also called hard x-ray photoelectron spectroscopy (HAXPES).[33] In particular, while soft x-ray PES has a probing depth of ~10–15 Å, HAXPES provides bulk-sensitive electronic structure with a probing depth of ~80–100 Å.[34] HAXPES also allows high resolution and high throughput for hard x-ray valence band studies in spite of low-ionization cross sections,[35] and the state of the art is best exemplified by a recent study of valence band dispersions using HAXPES.[36] It has also provided very interesting results and deep insights into a variety of materials.[27,28,30,33,35–41] This study provides the link between core-level spectra, valence band states, bonding changes, and the role of strong correlations on the electronic structure of ruthenate pyrochlores. After investigating the T-dependent electronic structure of $Tl_2Ru_2O_7$ and $Hg_2Ru_2O_7$ as typical examples of MITs, we then compare the applicability of the method to other compounds. The studies show the equivalence of screening from coherent states of the DMFT calculation[31] and the nonlocal screening of multisite calculations[32] in terms of changes in the experimental core-level and valence band spectra. Thus, bulk-sensitive photoelectron spectroscopy combined with configuration-interaction (CI) calculations provides a general and reliable method to quantify changes in the ionicity, covalency, and metallicity of correlated compounds.

II. SAMPLE PREPARATION, CHARACTERIZATION, AND EXPERIMENTAL DETAILS

Polycrystalline samples of $Tl_2Ru_2O_7$ and $Hg_2Ru_2O_7$ were synthesized using a high-pressure (4 GPa) cubic-anvil apparatus, as detailed in Ref. 24. The $Tl_2Ru_2O_7$ and $Hg_2Ru_2O_7$ samples were characterized for electrical resistivity $\rho(T)$,

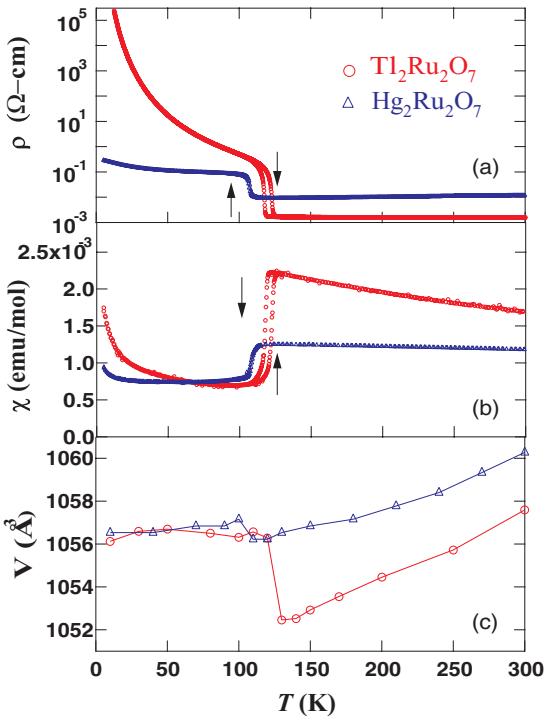

FIG. 2. (Color online) (a) Electrical resistivity ρ, (b) magnetic susceptibility χ, and (c) pseudocubic unit-cell volume V of $Tl_2Ru_2O_7$ and $Hg_2Ru_2O_7$, plotted as a function of temperature T. The first-order nature of the transitions in $\rho(T)$ and $\chi(T)$ is clear from the hysteresis seen in the data.

magnetic susceptibility $\chi(T)$, and crystal structure using x-ray diffraction (XRD) as a function of T, and the results are shown in Figs. 2(a)–2(c). The sharp first-order transitions in $\rho(T)$ and $\chi(T)$ seen in Figs. 2(a) and 2(b) (T_{MIT} =125 K and T_{MIT} = 108 K, for $Tl_2Ru_2O_7$ and $Hg_2Ru_2O_7$, respectively) are in very good agreement with earlier work and confirm the high quality of the samples.[10,23,24] Note also that both the compounds show a jump in the cell volume (V) at T_{MIT}, below which the volume stays essentially constant in the insulating phase [Fig. 2(c)], but the jump in $Hg_2Ru_2O_7$ is very small compared to that in $Tl_2Ru_2O_7$. The high-T phase is cubic in both compounds. While the low-T phase is orthorhombic in $Tl_2Ru_2O_7$ and triclinic in $Hg_2Ru_2O_7$, the low-temperature phase cell volumes are nearly the same. The effective magnetic moments estimated from the high-T susceptibility data indicate a $\mu_{eff} \sim 2.8\ \mu_B$ and $\mu_{eff} \sim 3.7\ \mu_B$ for $Tl_2Ru_2O_7$ and $Hg_2Ru_2O_7$, respectively, thus confirming spin-only values of $S = 1 (=2.76\ \mu_B)$ and $S = \frac{3}{2} (=3.87\ \mu_B)$ for the two compounds.[10,23,24] From high-temperature magnetic susceptibility measurements, the estimated Curie-Weiss temperature θ is large and negative for both $Tl_2Ru_2O_7$ and $Hg_2Ru_2O_7$, indicative of strongly antiferromagnetic nearest-neighbor interactions. The estimated $\theta \sim -950$ K for $Tl_2Ru_2O_7$ (Ref. 10), while for $Hg_2Ru_2O_7$, Klein *et al.*[23] estimated $\theta \sim -1700$ K, while our samples indicate a value of $\theta \sim -2700$ K.[24] These values of θ in relation to T_{MIT} (=125 and 108 K, for $Tl_2Ru_2O_7$ and $Hg_2Ru_2O_7$, respectively) indicate a large value of the frustration index f, defined as $f = \theta / T^*$, where T^* is the ordering temperature.[42] The estimated frustration indices are $f \sim 8$ for $Tl_2Ru_2O_7$ and $f \sim 15$–25 for $Hg_2Ru_2O_7$. In comparison, $Gd_2Ti_2O_7$ and $Gd_2Sn_2O_7$ exhibit a frustration index $f = 10$ and are considered very good examples of highly frustrated systems undergoing long-range order.[43] Here, the Gd^{3+} ion with a half-filled $4f$ shell and zero orbital momentum is considered to be the best example of a Heisenberg spin system on a pyrochlore lattice. While the f values are comparable for the Gd-based and ruthenate pyrochlores, the absolute values of θ and T^* in $Tl_2Ru_2O_7$ and $Hg_2Ru_2O_7$ are nearly 100 times larger than for $Gd_2Ti_2O_7$ and $Gd_2Sn_2O_7$ ($\theta = 10$ K and $T^* \approx 1$ K).[43] Interestingly, it was shown that $Tl_2Ru_2O_7$ exhibits $S = 1$ Haldane spin chains with a spin gap of about 11 meV ($\approx T_{MIT} = 125$ K), as reported from neutron scattering.[10] In contrast, the spin structure of $Hg_2Ru_2O_7$ is very complex, with NMR measurements[44] indicating four different types of Ru sites in the insulating phase, while μsR experiments indicate evidence for nearly commensurate magnetic order.[45] While this study using photoelectron spectroscopy can not address the magnetic structure, as will be discussed in the following, we could determine a charge gap of ~200 meV for $Tl_2Ru_2O_7$ and 160 meV for $Hg_2Ru_2O_7$ in the density of states (see Fig. 8 and related discussions). Our result indicates that the charge gaps (200 and 160 meV) are much larger than the spin gap (11 meV) known from neutron scattering for $Tl_2Ru_2O_7$, and the magnetic ordering temperature (108 K ≈ 9 meV) for $Hg_2Ru_2O_7$. We attribute the difference in the spin and charge gaps to frustration effects and fractionalization in the pyrochlore structure, as is predicted by theoretical studies.[46,47] However, it is also noted that frustration effects in magnetic properties leading to a quantum spin liquid (absence of magnetic ordering) are low-energy phenomena observed only at very low temperatures (<10 K). In the following, we describe the photoemission spectroscopy of the pyrochlore ruthenates and clarify the role of strong electron-electron correlations on its electronic structure, with implications on bonding and properties.

HAXPES measurements were carried out using an incident beam energy of $h\nu = 7.94$ keV and a Gammadata-Scienta analyzer at the RIKEN beamline BL29XU, and the instrumentation was reported earlier.[35] The total energy resolution was 230 meV (full-width at half-maximum of a Gaussian) for the present HAXPES experiments, as determined from a fit to the Fermi edge of gold. In addition, the energy position accuracy of the Fermi edge is better than ±10 meV. The high accuracy of the energy position at a high kinetic energy (~7.93 keV) is crucial to measure small energy gaps (~100 meV, see Fig. 8) and is due to the combination of the crystal optics used for monochromatizing the incident photon source, and the stability of the high-resolution energy analyzer. Samples were cleaved *in situ* for all the spectroscopy experiments. The sample temperature was controlled using a liquid-He flow type cryostat. Temperature-dependent changes were reproducibly obtained upon temperature cycling.

III. RESULTS AND DISCUSSIONS

We first discuss the HAXPES O 1s core-level spectra of $Tl_2Ru_2O_7$ and $Hg_2Ru_2O_7$, obtained at temperatures above and below T_{MIT} and shown in Figs. 3(a) and 3(b). The spectra show a clean single-peak feature. Since it is known that

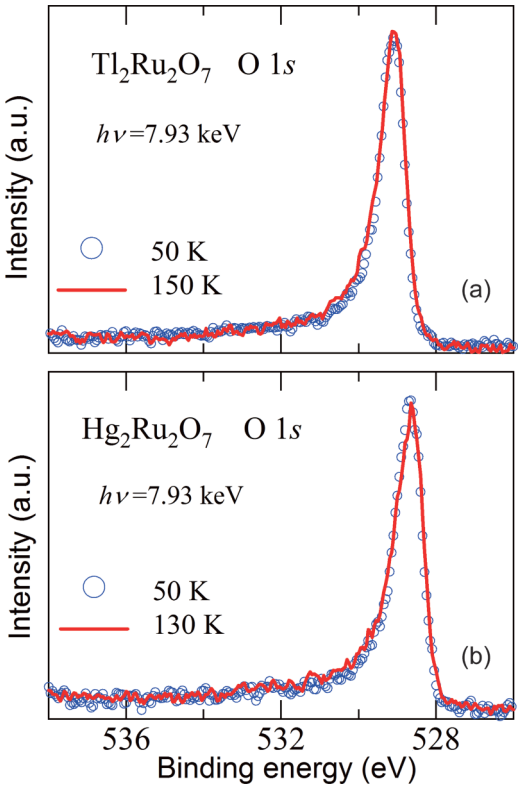

FIG. 3. (Color online) (a) and (b) show the O 1*s* core-level spectra of $Tl_2Ru_2O_7$ (T_{MIT} = 125 K) and $Hg_2Ru_2O_7$ (T_{MIT} = 108 K), respectively, measured for temperatures above and below the transition temperature T_{MIT}. The spectra show negligible change above and below T_{MIT}.

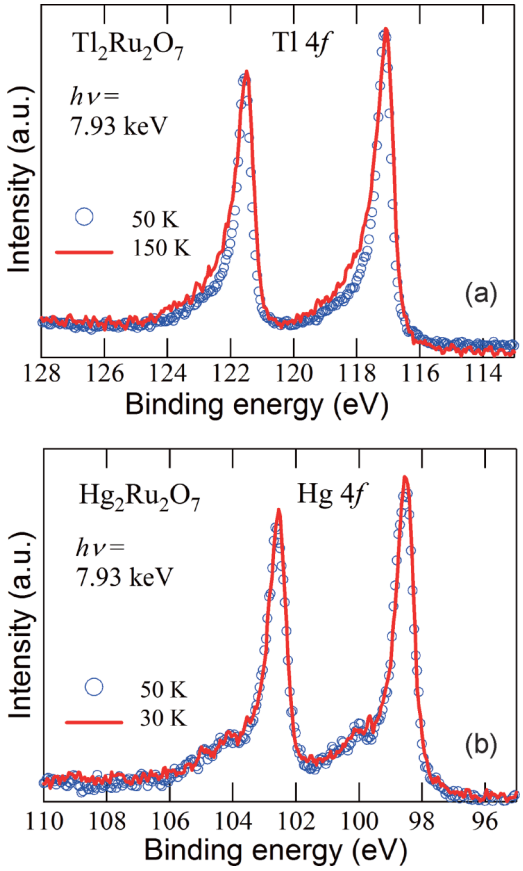

FIG. 4. (Color online) (a) and (b) show the Tl 4*f* and Hg 4*f* core-level spectra of $Tl_2Ru_2O_7$ and $Hg_2Ru_2O_7$, respectively, measured for temperatures above and below the T_{MIT}. The spectral features show negligible change above and below T_{MIT}.

surface effects or contaminants result in a high binding-energy (BE) satellite in oxides,[48] the single-peak spectra obtained here confirm absence of surface effects and contaminants. For $Tl_2Ru_2O_7$, the O 1*s* peak is at a BE of 529.1 eV, while for $Hg_2Ru_2O_7$, it occurs at 528.65 eV. The BEs are typical of metal oxides. The difference in binding energies originates from a chemical shift of Ru^{4+} and Ru^{5+} as is confirmed from Ru 3*d* core-level spectra (Fig. 5) of $Tl_2Ru_2O_7$ and $Hg_2Ru_2O_7$, which show a corresponding but opposite shift in BEs, and discussed in detail below. Note that since the Ru-O bond distances and the unit-cell volumes are nearly the same in the low-temperature phase [see Fig. 2(c)], it rules out the possibility of a Madelung potential origin[49] for the difference in binding energies of the O 1*s* peaks. This is because a Madelung potential origin would indicate that the nearest-neighbor metal-ligand distances should be different in $Tl_2Ru_2O_7$ and $Hg_2Ru_2O_7$, in contrast to known experimental results of the crystal structure [Refs. 10,23,24 and Fig. 2(c)]. Further, the spectra do not show any temperature dependence across the MIT, and this also rules out T-dependent changes in the chemical potential[50] for the metallic and insulating phases. This suggests that the Fermi level or chemical potential is fixed to the middle of the gap for the insulating phase.

Figures 4(a) and 4(b) show the Tl 4*f* and Hg 4*f* core-level spectra of $Tl_2Ru_2O_7$ and $Hg_2Ru_2O_7$. Here again the $4f_{7/2}$ and $4f_{5/2}$ levels show single peaks indicative of a well-defined *A*-site valence. In $Tl_2Ru_2O_7$, the spectra are typical of Tl^{3+} [BEs: 117.1 and 121.5 eV; spin-orbit splitting (or SOS): 4.4 eV]. The SOS and BEs for Tl 4*f* in $Tl_2Ru_2O_7$ are consistent with the main peaks in Tl_2O_3.[51] The Hg 4*f* spectra are assigned to that of Hg^{2+} in $Hg_2Ru_2O_7$ (BEs: 98.5 and 102.55 eV; SOS: 4.05 eV). While the SOS in $Hg_2Ru_2O_7$ matches with that of HgO, the Hg 4*f* BEs are 2 eV lower than in HgO.[51] We attribute this difference to the fact that HgO has a band gap of 2 eV. This is borne out by the observation that the Hg 5*d* states (see Fig. 7) are also positioned at 2 eV lower BE compared to HgO. The negligible temperature dependence of the peak binding energies and spectral shapes across T_{MIT} in Tl 4*f* and Hg 4*f* states suggest that the *A*-site electronic states are not primarily responsible for the MIT, although the *A*-site ions play a role in the coupled structural properties.[52,53] In turn, these results suggest changes in Ru-derived states would reflect the MIT, as discussed in the next paragraph.

Figures 5(a) and 5(b) show the HAXPES Ru 3*d* core-level spectra (symbols) of $Tl_2Ru_2O_7$ and $Hg_2Ru_2O_7$, obtained above and below T_{MIT}. The Ru 3*d* core-level spectra show very clear changes above and below T_{MIT} for $Tl_2Ru_2O_7$ and $Hg_2Ru_2O_7$. In the metallic phase, for both the compounds, the spectra consist of two main broad features for each of the $3d_{5/2}$ and the $3d_{3/2}$ states. The binding energies (BEs) of the $3d_{5/2}$ main features are 280.9 and 281.9 eV for $Tl_2Ru_2O_7$ and 281.5 and 282.4 eV for $Hg_2Ru_2O_7$. The relatively higher and lower BE

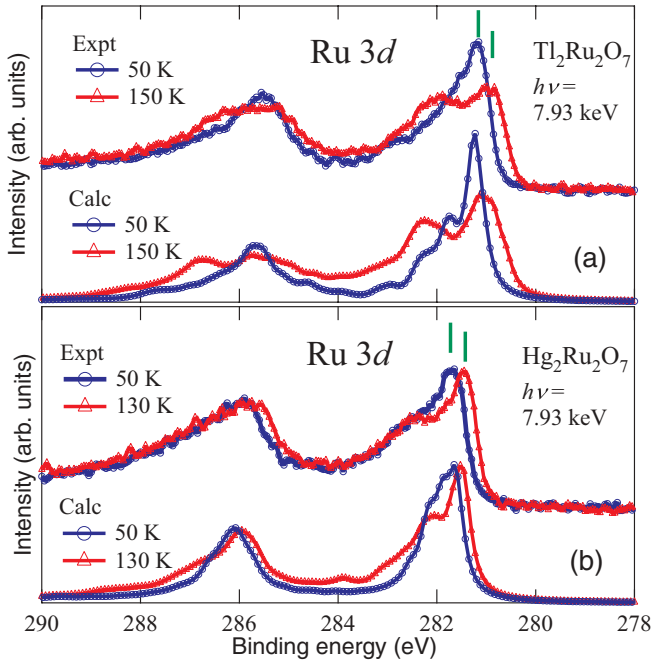

FIG. 5. (Color online) Core-level experimental and calculated spectra: (a) and (b) show the Ru $3d$ core-level spectra of $Tl_2Ru_2O_7$ and $Hg_2Ru_2O_7$, respectively, for temperatures above and below the T_{MIT} compared with single-impurity Anderson model calculations including ligand- and metallic-screening channels. The experimental spectra show clear changes above and below T_{MIT} for both the compounds which are reproduced by the CI calculations. The insulating phase calculated spectra are obtained by setting the metallic-screening energy $V^* = 0$, keeping all other parameters fixed as for the metal phase. Green tick marks show equal binding energy shifts in the metal and insulating phases for $Tl_2Ru_2O_7$ and $Hg_2Ru_2O_7$, which are indicative of negligible changes in the ionic bonding components.

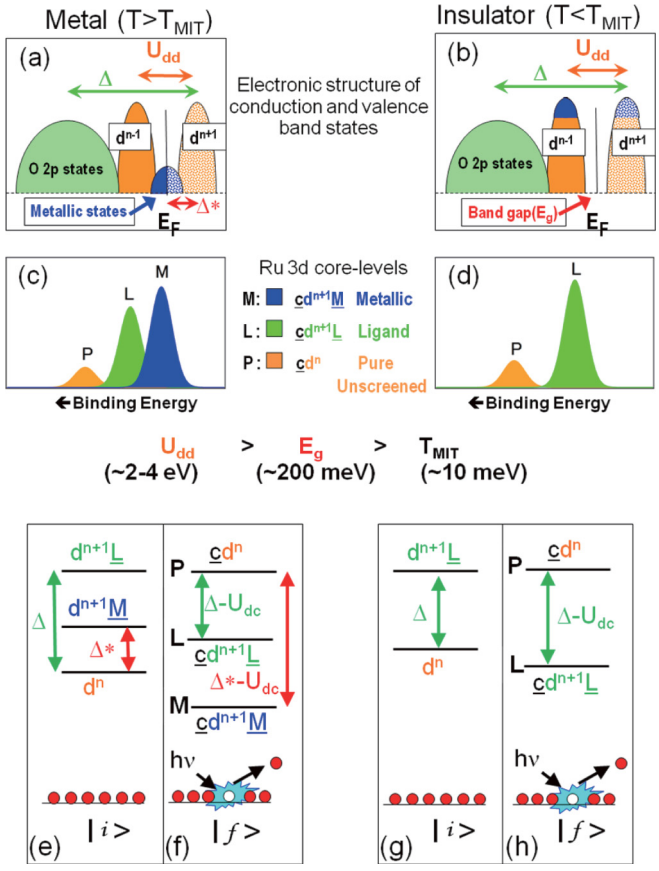

FIG. 6. (Color online) Schematics of the electronic structure across the MIT in the pyrochlore ruthenates: The valence and conduction band states for Mott-Hubbard (a) metal ($T > T_{MIT}$) and (b) insulating ($T < T_{MIT}$) phase of $Hg_2Ru_2O_7$ with $\Delta > U_{dd}$. The MIT occurring at $T_{MIT} = 108$ K (~10 meV) results in gap formation E_g (~160 meV) and spectral weight transfer on ~eV energy scale associated with onsite Coulomb energy U_{dd}. Panels (c) and (d) show the spectral assignments of the Ru $3d$ core-level spectra for the metal and insulating phases, respectively, in terms of $\underline{c}d^n$, $\underline{c}d^{n+1}\underline{L}$, and $\underline{c}d^{n+1}\underline{M}$ states with $\Delta < U_{dc}$, where $\underline{c}$ is the core hole and U_{dc} is the core-hole potential operative only in the final state. Panels (e), (f) for $T > T_{MIT}$ and (g), (h) for $T < T_{MIT}$ show the the initial (|i⟩) states and their rearrangement in the final (|f⟩) states due to the presence of a core hole $\underline{c}$ in the Ru $3d_{5/2}$ core level. The metallic-screened peak M seen in the high-temperature metallic phase in panel (c) gets quenched in the low-temperature insulating phase of panel (d).

peaks are often discussed as the poorly screened (shake-up), and well-screened (shake-down) features, respectively.[6,54,55] The difference in BEs of $Tl_2Ru_2O_7$ and $Hg_2Ru_2O_7$ is attributed to the chemical shift of Ru^{4+} and Ru^{5+}. Chemical shift due to valency was originally reported by HAXPES using a laboratory source and is a reliable fingerprint of ionic configurations.[56,57] An opposite chemical shift in the BEs of the O $1s$ peaks was discussed above for $Tl_2Ru_2O_7$ and $Hg_2Ru_2O_7$. The Ru^{5+} BE (281.5 eV) lies between the reported values[57] of nominal Ru^{4+} (280.8 eV) and Ru^{6+} (282.5 eV). On reducing temperature below T_{MIT}, the spectra become narrower for both $Tl_2Ru_2O_7$ and $Hg_2Ru_2O_7$. The narrowing in the insulating phase rules out charge disproportionation, which is expected to make the peaks broader. The corresponding insulating phase BEs are 281.25 and 281.75 eV for the main peaks, which can be described as consisting of essentially one broad structured peak. The structure within each of the Ru $3d$ peaks is due to the atomic multiplets of a single configuration (d^4 for $Tl_2Ru_2O_7$ and d^3 for $Hg_2Ru_2O_7$), as confirmed by the model calculations shown in Fig. 5 (full lines) and discussed below. Since the BEs are a measure of the ionicity of Ru ions, and the obtained BE shifts for Ru^{4+} and Ru^{5+} in the metallic and insulating phases are equal [see green tick marks in Figs. 5(a) and 5(b)], it indicates that the ionic bonding components do not change across the MIT in $Tl_2Ru_2O_7$ and $Hg_2Ru_2O_7$.

As a means to analyze the rich structure in the Ru $3d$ core-level spectra of $Tl_2Ru_2O_7$ and $Hg_2Ru_2O_7$ above and below T_{MIT}, we have carried out CI calculations of the core-level spectra based on the single-impurity Anderson model (SIAM).[58] The SIAM calculations, as well as the related cluster-model calculations,[59] have been very successful in explaining the relative intensities and energy positions of core-level spectral features in strongly correlated $3d$ and $4f$ compounds.[60] The calculations are carried out as follows: the initial or ground state of an MO_6 cluster is described as a linear combination of an orthonormal set of basis states. The

basis states are d^n, $d^{n+1}\underline{L}$, $d^{n+1}\underline{M}$, etc., where d^n depends on the valency and includes the atomic multiplets of the pure d^n configuration. Accordingly, for Ru^{4+}, $d^n = d^4$, and for Ru^{5+}, $d^n = d^3$. A hole in the ligand band is denoted $\underline{L}$, and $d^{n+1}\underline{L}$ is a state obtained from d^n by ligand screening. Similarly, $\underline{M}$ denotes a hole in the metallic coherent band and $d^{n+1}\underline{M}$ is a state obtained from d^n by metallic screening. While the standard SIAM calculation considers screening from one band, in the present case we have considered the ligand band and the metallic coherent band as independent screening channels. The metallic screening is active only in the metal phase and is forbidden in the insulating phase, as the metallic states get quenched due to gap formation in the insulator. The final or excited states are described as a linear combination of the same states with a core hole ($\underline{c}$), which is the source of an attractive interaction U_{dc} operative only in the final state. While states of the type $d^{n+2}\underline{L}^2$, $d^{n+2}\underline{M}^2$, etc., are allowed, it was found that these are high-energy states with negligible spectral weight, and could be neglected. The basis states interact via the Anderson Hamiltonian which includes the bare energies [Δ is the charge-transfer energy; Δ^* is the energy between the metallic states and upper Hubbard band, see Figs. 6(a) and 6(b)], the onsite Coulomb energy U_{dd}, the crystal-field splitting (10 Dq) at the Ru site, and V (V^*) is the hybridization strength of Ru $4d$ with the ligand p (metallic coherent) states. The eigenvalues of the initial and final states are obtained by a numerical diagonalization and the intensities of the features are calculated in the sudden approximation for a trial set of parameters. The calculated spectra are compared to the experimental spectra to obtain the best fit by varying the parameters. The model has been fully described in Ref. 27. The starting parameters can be chosen based on well-established chemical trends: U_{dd} is an atomic parameter given by the ionization energy and electron affinity, and is known to change systematically from the early to late transition metals.[25,61] Δ, the charge-transfer energy, is determined by the electronegativity difference between the cation and anion, and reduces on increasing the oxidation state.[25] In a series of isostructural compounds, the hybridization strength is proportional to the metal-ligand bond distance.[62] In addition, the spin configuration follows Hund's rules, and from the experimentally obtained effective magnetic moments, it is generally possible to determine an appropriate (10 Dq) compatible with the known low- or high-spin configuration.[60] Schematics of the valence band energy-level scheme for the cases of Mott-Hubbard metal and insulator are shown in Figs. 6(a) and 6(b). For the measured Ru $3d$ core-level photoelectron spectra of $Tl_2Ru_2O_7$ and $Hg_2Ru_2O_7$, Figs. 6(c) and 6(d) show the obtained spectral feature assignments for the metal and insulating phases, respectively, as detailed below. Figures 3(e) to 3(h) show corresponding Ru $3d$ core-energy-level schemes of the initial ($|i\rangle$) states and their rearrangement in the final ($|f\rangle$) states due to the core hole $\underline{c}$ created by the photoelectron process.

The results of the SIAM model calculations for $Tl_2Ru_2O_7$ and $Hg_2Ru_2O_7$ are shown in Figs. 5(a) and 5(b) along with the experimental spectra. We could obtain a reasonably good fit to the experimental spectra using the parameters listed in Table I. A particular noteworthy feature of the calculations is that the same set of parameters is used to obtain the metallic and insulating phase spectra, with the only change being that the parameter V^* is set to 0 for the insulating phase calculation. Further, the best fit required a Ru onsite Coulomb energy of $U_{dd} = 3$ eV for $Tl_2Ru_2O_7$ and $U_{dd} = 4$ eV for $Hg_2Ru_2O_7$. Although U_{dd} is considered an atomic parameter, a comparable variation of U_{dd} is known for other ruthenate compounds.[31,32] The obtained parameters, specifically $U_{dd} < \Delta$, indicates that $Tl_2Ru_2O_7$ and $Hg_2Ru_2O_7$ are Mott-Hubbard systems. We have also analyzed the character of the features and find that, for the metal phase, the well-screened feature originates in dominantly $\underline{c}d^{n+1}\underline{M}$ states [$3d_{5/2}$ feature at 281.5 eV for $Hg_2Ru_2O_7$ and 280.9 eV for $Tl_2Ru_2O_7$ in Fig. 5; label M in Fig. 6(c)]. For $Hg_2Ru_2O_7$, the $\underline{c}d^{n+1}\underline{L}$ states are at about 1 eV higher binding energy [at 282.4 eV in Fig. 5; label L in Fig. 6(c)] and the $\underline{c}d^n$ states are weak features at 284 eV in Fig. 5 [label P in Fig. 6(c)]. In contrast, the assignment of $\underline{c}d^{n+1}\underline{L}$ and $\underline{c}d^n$ features for $Tl_2Ru_2O_7$ are interchanged: the $\underline{c}d^n$ states are at 281.9 eV and the $\underline{c}d^{n+1}\underline{L}$ states are the weak features at ~283 eV in Fig. 5. This difference in assignment of features is due to the relative difference in the energy parameters Δ and U_{dc} required to simulate the spectra for $Tl_2Ru_2O_7$ ($\Delta > U_{dc}$) and $Hg_2Ru_2O_7$ ($\Delta < U_{dc}$), while $\Delta < U_{dd}$ for both compounds. A similar assignment holds for the insulating phase [Fig. 6(d)] but in the absence of $\underline{c}d^{n+1}\underline{M}$ metallic states.

It is noted that the Ru_4 multisite cluster calculations with orbital order reported[32] very similar results like the metal phase results of $Tl_2Ru_2O_7$ obtained here. However, for $Hg_2Ru_2O_7$, even in the absence of orbital ordering, the role of Ru-site correlations is analogous to that of $Tl_2Ru_2O_7$ from the present results. For the pyrochlores, it is known that the Ru-O-Ru bond angle shows a direct relationship with the crystal radii of the A-site cation[5–7,52,53,63] Consequently, the parameter V^* may be viewed upon as an effective Ru-O-Ru hopping strength of itinerant carriers, which sensitively depends on the Ru-O-Ru angle. Hence, the Ru $3d$ core-level spectra prove the role of metallic or coherent state screening in the metal phase which gets quenched in the insulating phase. Accordingly, just as the hybridization V corresponds to the covalent bonding energy associated with mixing p states with the Hubbard band d states,[59,60] by analogy, the characteristic energy V^* is associated with an effective metallicity which mixes the

TABLE I. Microscopic electronic parameters obtained for $Tl_2Ru_2O_7$ and $Hg_2Ru_2O_7$: Parameter values used to obtain the Ru $3d$ core-level calculated spectra matching the experiment. W_L, W_C are the ligand states and metallic states bandwidths. The remaining parameters are explained in the text. All the parameters have an error bar of ±10%.

Parameter (in eV)	$Tl_2Ru_2O_7$	$Hg_2Ru_2O_7$
Δ	7.0	4.5
Δ^*	0.1	0.1
U_{dd}	3.0	4.0
U_{dc}	3.8	5.4
10 Dq	2.5	3.8
W_L	5.0	5.0
W_C	0.5	0.3
V	2.2	2.0
V^*	0.55	0.94

coherent d states with the Hubbard band or incoherent d states [see Fig. 6(a)].

For $Tl_2Ru_2O_7$, we obtain $V = 2.2$ eV (=50.73 kcal/mol) and $V^* = 0.55$ eV (=12.60 kcal/mol), and for $Hg_2Ru_2O_7$, $V = 2.0$ eV (=46.12 kcal/mol) and $V^* = 0.94$ eV (=21.68 kcal/mol). Since V^* is significantly larger for $Hg_2Ru_2O_7$ compared to $Tl_2Ru_2O_7$, it suggests $Hg_2Ru_2O_7$ is more stable than $Tl_2Ru_2O_7$ in the high-temperature metallic phase. Although the formation enthalpies of pyrochlore ruthenates have not been reported, based on the A- and B-site crystal radii,[63] we compare with the trend known from a series of pyrochlore titanates.[64] The larger radius of A-site Hg^{2+} ion (1.14 Å) compared to Tl^{3+} (0.98 Å) and, simultaneously, the smaller radius of B-site Ru^{5+} (0.705 Å) compared to Ru^{4+} (0.76 Å) suggests that $Hg_2Ru_2O_7$ would be more stable than $Tl_2Ru_2O_7$ by about 5–10 kcal/mole. The estimated values of V and V^* are also consistent with recent results of GGA+U band-structure calculations[65] which concluded that $Hg_2Ru_2O_7$ is more delocalized compared to $Tl_2Ru_2O_7$. The suppression of V^* also shows that the transitions in both $Tl_2Ru_2O_7$ (with Ru^{4+}) and $Hg_2Ru_2O_7$ (with Ru^{5+}) are bandwidth-controlled Mott-Hubbard MITs, as was predicted theoretically in early work for Ru^{4+} pyrochlores.[52] A final proof of this is an actual measurement of the valence band spectra of $Tl_2Ru_2O_7$ and $Hg_2Ru_2O_7$.

Figures 7(a) and 7(b) show the HAXPES valence band spectra of $Tl_2Ru_2O_7$ and $Hg_2Ru_2O_7$ obtained above and below T_{MIT}. The spectra are normalized for area under the curve. For $Tl_2Ru_2O_7$, the valence band consists of the Tl $5d_{5/2}$ and $5d_{3/2}$ doublet at 12.1 and 14.2 eV BE, Tl 6s states mainly between 6–8 eV, a broad dominantly O 2p character band between ~1.5–6 eV, and the dominantly Ru 4d states mixed with O 2p states between 1.5 eV BE and E_F. $Hg_2Ru_2O_7$ shows the Hg $5d_{5/2}$ and $5d_{3/2}$ derived features occurring between 6–12 eV with peaks at 6.7 and 8.5 eV binding energy, a broad O 2p character band between ~1.5 to 6 eV, while the dominantly Ru 4d states mixed with O 2p states occur at BEs below 1.5 eV. These assignments are based on band-structure calculations reported in the literature.[10,16,52,65,66]

For $Hg_2Ru_2O_7$, a recent local density approximation (LDA) calculation[66] showed that the Hg 5d states are affected by spin-orbit coupling (SOC), but the SOC does not modify states near E_F. The observed relative intensities and widths of the Hg 5d states are consistent with these calculations, indicating the role of SOC, but the peaks are positioned at about 1 eV higher BE than the calculations. From LDA + DMFT calculations,[66] the same study concluded that $Hg_2Ru_2O_7$ can undergo an orbital selective Mott-Hubbard transition in the Ru 4d states at E_F. For $Tl_2Ru_2O_7$, while earlier calculations[16] discussed the possible role of Tl 6s states for the MIT, the recent LDA + U calculation[10] showed a Ru 4d orbital ordering induced MIT for $Tl_2Ru_2O_7$. In particular, it is noted that the Tl 5d and 6s as well as the Hg 5d states show negligible T-dependent changes in the experimental valence band spectra. Also, the Tl and Hg 4f core-level spectra did not show T-dependent spectral features, as discussed earlier.

While the large-energy-scale spectra do not show changes below and above T_{MIT}, we plot the near E_F spectra on an expanded scale in Figs. 8(a) and 8(b). For the high-temperature phase, the leading edge matches the gold spectrum measured

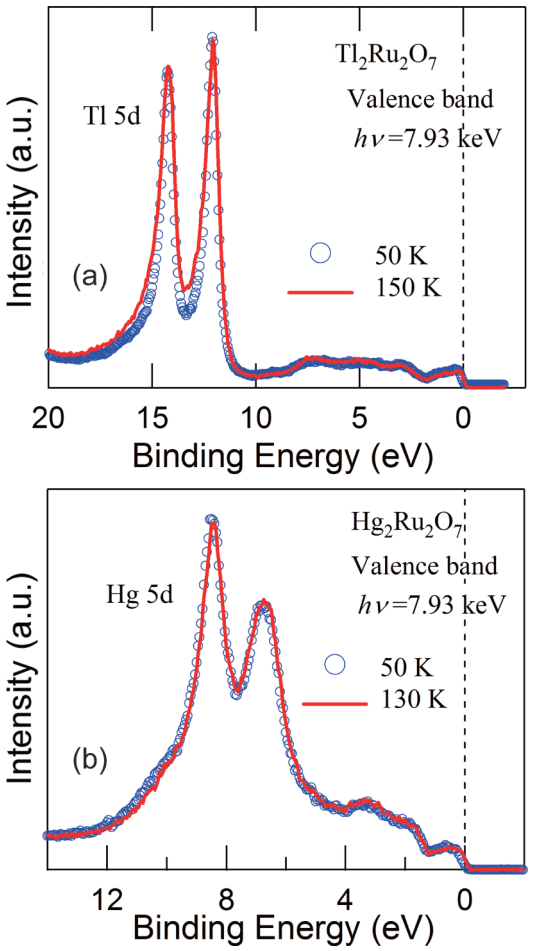

FIG. 7. (Color online) Bulk-sensitive hard x-ray (hν = 7.93 keV) valence band spectra of (a) $Tl_2Ru_2O_7$ and (b) $Hg_2Ru_2O_7$ above and below the T_{MIT}. The spectra show negligible changes above and below T_{MIT} for both compounds over the wide energy scale.

under the same conditions, as a reference. On reducing temperature below T_{MIT}, we observe a clear shift of the leading edge. This is evidence of a gap formation across T_{MIT} in the Ru 4d states. The shift in the leading edge is about 100 meV for $Tl_2Ru_2O_7$ and is exactly half the total gap of about 200 meV obtained from optical spectroscopy.[67] For $Hg_2Ru_2O_7$, we obtain a slightly smaller shift of about 80 meV and, if we assume this to be half the gap (in the absence of optical data), it suggests a full gap of 160 meV for $Hg_2Ru_2O_7$. The small gap formation leads to a finite spectral weight transfer, but over a large scale of ~1 eV in the valence band, confirming the role of strong correlations in the MIT. The T-dependent valence band results thus confirm the validity of the SIAM calculations for the changes seen in the Ru 3d core-level spectra. A recent GGA + U band-structure calculation[65] showed a metallic ground state for $Hg_2Ru_2O_7$. However, when a noncollinear magnetic structure was assumed, as was recently proposed by NMR studies,[44] the GGA + U results showed a small gap of 0.1 eV. Thus, strong correlations and a noncollinear magnetic structure are deemed necessary to explain the electronic structure of $Hg_2Ru_2O_7$, while $Tl_2Ru_2O_7$ is best explained as a correlated system with orbital ordering.

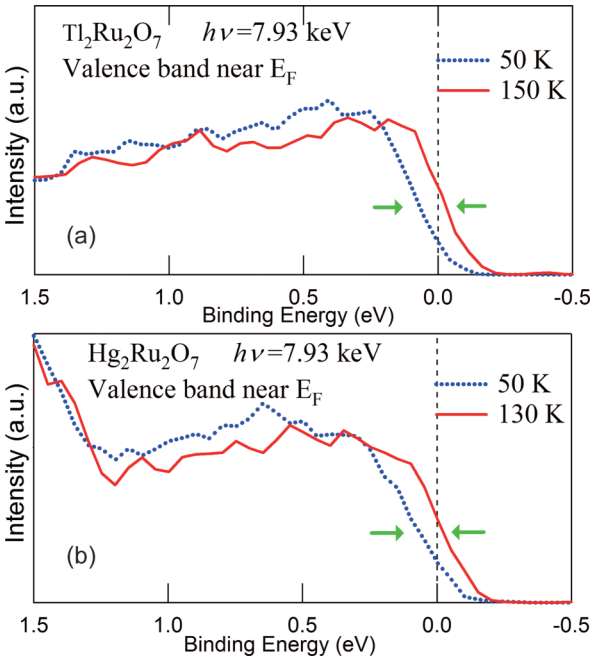

FIG. 8. (Color online) Bulk-sensitive hard x-ray ($h\nu = 7.93$ keV) near E_F valence band spectra for (a) $Tl_2Ru_2O_7$ and (b) $Hg_2Ru_2O_7$, above and below the T_{MIT}, plotted on an expanded binding-energy scale. The spectra are normalized for area under the curve. The spectra show clear shifts of the leading edge above and below T_{MIT} for both the compounds, indicative of gap formation (green arrows) across T_{MIT}.

The identification of the roles of covalency and metallicity across the MITs in $Tl_2Ru_2O_7$ and $Hg_2Ru_2O_7$ allows us to systematize the same for a series[27,30,41,68–71] of strongly correlated TMCs undergoing temperature- and doping-dependent MITs. In Table II, we list V and V^* obtained in kcal/mol from these studies. The list includes V_2O_3, CrN, the CMR manganese oxides, the high-T_c hole- and electron-doped copper-oxide superconductors, etc. Table II shows that the ratio $V : V^* =$

TABLE II. Covalent bonding and metallic-screening energies of TMCs and some standard bonding energies for comparison.

Compound	V^* (kcal/mol)	V (kcal/mol)	Ref. No.
$Tl_2Ru_2O_7$	12.60	50.73	This work
$Hg_2Ru_2O_7$	21.68	46.12	This work
Ti_4O_7	20.06	66.88	68
VO_2	11.07	55.34	69
V_2O_3	17.29	66.88	27
CrN	17.53	62.26	70
$La_{0.8}Sr_{0.2}MnO_3$	9.80	67.80	41
$La_{0.85}Ba_{0.15}MnO_3$	9.22	67.80	71
$La_{1.85}Sr_{0.15}CuO_4$	28.83	86.48	30
$Nd_{1.85}Ce_{0.15}CuO_4$	41.51	80.71	30
Standard bonds			
C-H bond		99	1
C-C bond		83	1
C-N bond		73	1
Hydrogen bonding		~5	1
van der Waals		~1	1

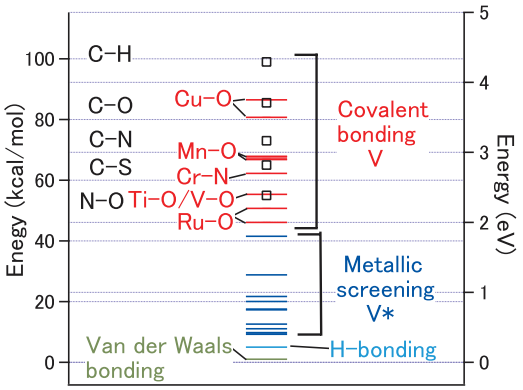

FIG. 9. (Color online) The obtained metallic-screening energies ($V^* \sim 10$–40 kcal/mol), which effectively mix the coherent and incoherent d states, form a distinct class lying between the stronger metal-ligand covalent bonding ($V \sim 45$–90 kcal/mol) and the weaker van der Waals and hydrogen bonding ~1–5 kcal/mol. The squares indicate values for standard heteronuclear covalent bonds C-H, C-O, etc.

$\sim 51 \sim 13$ kcal/mol for $Tl_2Ru_2O_7$, and ~67:~22 kcal/mol for $Hg_2Ru_2O_7$. Thus, the ruthenates fall in the same class as the early TMCs such as Ti_4O_7 (the Magneli compound), V_2O_3, and VO_2 with $V:V^* = 45$–$65 : 10$–20 kcal/mol. We can accordingly conclude that the ruthenates definitively undergo a Mott-Hubbard type of MIT as a function of temperature like the early TMCs. CrN, which undergoes a magnetostructural transition coupled to a MIT also gives comparable values of V and V^*, while the metallic phase of the doped manganese perovskites show the weakest V^*. In contrast, the high-T_c copper-oxide-based superconductors belong to the charge-transfer type of correlated compounds[30] and show significantly larger values of V (~80/85 kcal/mol) and V^* (~30/40 kcal/mol). The obtained values of V are very consistent with covalent metal-ligand bond energies[72] known for TMCs across the series from thermochemical data, which lie between ~2–3 eV (~46–69 kcal/mol). It is important to note that the metal-ligand bonding energies V (~45–90 kcal/mol) are also comparable with standard heteronuclear covalent bonds such as C-H, C-O, C-N, etc., as listed in Table II, while the metallic-screening energies V^* form a weaker class (~10–40 kcal/mol). Nonetheless, V^* is stronger than hydrogen bonding in water (~5 kcal/mol), as well as typical van der Waals bonding (~1 kcal/mol). It is noted that thermochemical methods can not distinguish bonding changes associated with metal-insulator transitions as is possible with the present method. Figure 9 summarizes the obtained results and classifies V^* as lying between the stronger covalent bonding and weaker van der Waals and hydrogen bonding.

IV. CONCLUSIONS

In conclusion, our study indicates validity of a general method to quantify covalency and metallicity in strongly correlated compounds across the transition-metal series, and gives the result that temperature- and doping-induced MITs are driven by similar changes: the ionic and covalent bonding do not change across the MIT, while the metallicity gets quenched

in the insulating phase. The study reveals three energy scales of the electronic structure of $Tl_2Ru_2O_7$ and $Hg_2Ru_2O_7$: (a) spectral transfer changes occur over the largest (∼eV) energy scale, (b) the band-gap energies or charge gaps ($E_g \sim 160$–200 meV) are intermediate, and (c) the lowest-energy scale corresponds to the transition temperature T_{MIT}, the known spin gap (128 K ∼ 11 meV ∼ $T_{MIT} = 125$ K) of $Tl_2Ru_2O_7$ and magnetic ordering temperature ($T_{MIT} = 108$ K ∼ 9 meV) of $Hg_2Ru_2O_7$. We hope the method will find widespread use as a standard tool to characterize bonding in correlated compounds, thereby providing an understanding of their properties as well as valuable inputs for design strategies in material synthesis.

[1] L. Pauling, *The Nature of the Chemical Bond and the Stucture of Molecules and Crystals: An Introduction to Modern Structural Chemistry*, 3rd ed. (Cornell University Press, Ithaca, 1960).

[2] J. G. Bednorz and K. A. Mueller, Z. Phys. B. **64**, 189 (1986).

[3] G. H. Jonker and J. H. van Santen, Physica (Amsterdam) **16**, 337 (1950).

[4] E. Canadell and M. H. Whangbo, Chem. Rev. **91**, 965 (1991).

[5] A. W. Sleight, Inorg. Chem. **7**, 1704 (1968).

[6] P. A. Cox, R. G. Egdell, J. B. Goodenough, A. Hamnett, and C. C. Naish, J. Phys. C: Solid State Phys. **16**, 6221 (1983).

[7] M. A. Subramaniam, G. Aravamudan, and G. V. Subba Rao, Prog. Solid State Chem. **15**, 55 (1983).

[8] Y. Shimakawa, Y. Kubo, and T. Manako, Nature (London) **379**, 53 (1996).

[9] A. P. Ramirez, A. Hayashi, R. J. Cava, R. Siddharthan, and B. S. Shastry, Nature (London) **399**, 333 (1999).

[10] S. Lee, J.-G. Park, D. T. Adroja, D. Khomskii, S. Streltsov, K. A. McEwen, H. Sakai, K. Yoshimura, V. I. Anisimov, D. Mori, R. Kanno, and R. Ibberson, Nat. Mater. **5**, 471 (2006).

[11] M. Hanawa, Y. Muraoka, T. Tayama, T. Sakakibara, J. Yamaura, and Z. Hiroi, Phys. Rev. Lett. **87**, 187001 (2001).

[12] A. O. E. Animalu, Phys. Rev. B **10**, 4964 (1974).

[13] R. G. Moore, J. Zhang, V. B. Nascimento, R. Jin, J. Guo, G. T. Wang, Z. Fang, D. Mandrus, and E. W. Plummer, Science **318**, 615 (2007).

[14] P. Khalifah, R. Osborn, Q. Huang, H. W. Zandbergen, R. Jin, Y. Liu, D. Mandrus, and R. J. Cava, Science **297**, 2237 (2002).

[15] D. J. Singh, Phys. Rev. B **55**, 313 (1997).

[16] F. Ishii and T. Oguchi, J. Phys. Soc. Jpn. **69**, 526 (2000).

[17] J. Okamoto, T. Mizokawa, A. Fujimori, T. Takeda, R. Kanno, F. Ishii, and T. Oguchi, Phys. Rev. B **69**, 035115 (2004).

[18] C. Felser, G. H. Fecher, and B. Balke, Angew. Chem. Int. Ed. **46**, 668 (2007).

[19] W. P. Anderson, J. K. Burdett, and P. T. Czech, J. Am. Chem. Soc. **116**, 8808 (1994).

[20] J. S. Schon, Angew. Chem. Int. Ed. **34**, 1081 (1995).

[21] Antoine Georges, Gabriel Kotliar, Werner Krauth, and Marcelo J. Rozenberg, Rev. Mod. Phys. **68**, 13 (1996).

[22] Masatoshi Imada, Atsushi Fujimori, and Yoshinori Tokura, Rev. Mod. Phys. **70**, 1039 (1998).

[23] W. Klein, R. K. Kremer, and M. Jansen, J. Mater. Chem. **17**, 1356 (2007).

[24] A. Yamamoto, P. A. Sharma, Y. Okamoto, A. Nakao, H. Aruga Katori, S. Niitaka, D. Hashizume, and H. Takagi, J. Phys. Soc. Jpn. **76**, 043703 (2007).

[25] J. Zaanen, G. A. Sawatzky, and J. W. Allen, Phys. Rev. Lett. **55**, 418 (1985).

[26] S.-K. Mo, J. D. Denlinger, H.-D. Kim, J.-H. Park, J. W. Allen, A. Sekiyama, A. Yamasaki, K. Kadono, S. Suga, Y. Saitoh, T. Muro, P. Metcalf, G. Keller, K. Held, V. Eyert, V. I. Anisimov, and D. Vollhardt, Phys. Rev. Lett. **90**, 186403 (2003).

[27] M. Taguchi, A. Chainani, N. Kamakura, K. Horiba, Y. Takata, M. Yabashi, K. Tamasaku, Y. Nishino, D. Miwa, T. Ishikawa, S. Shin, E. Ikenaga, T. Yokoya, K. Kobayashi, T. Mochiku, K. Hirata, and K. Motoya, Phys. Rev. B **71**, 155102 (2005).

[28] G. Panaccione, M. Altarelli, A. Fondacaro, A. Georges, S. Huotari, P. Lacovig, A. Lichtenstein, P. Metcalf, G. Monaco, F. Offi, L. Paolasini, A. Poteryaev, O. Tjernberg, and M. Sacchi, Phys. Rev. Lett. 2006, **97**, 116401 (2006); H. Fujiwara, A. Sekiyama, S.-K. Mo, J. W. Allen, J. Yamaguchi, G. Funabashi, S. Imada, P. Metcalf, A. Higashiya, M. Yabashi, K. Tamasaku, T. Ishikawa, and S. Suga, Phys. Rev. B **84**, 075117 (2011).

[29] A. Fujimori, E. Takayama-Muromachi, Y. Uchida, and B. Okai, Phys. Rev. B **35**, 8814 (1987); C. T. Chen, F. Sette, Y. Ma, M. S. Hybertsen, E. B. Stechel, W. M. C. Foulkes, M. Schluter, S-W. Cheong, A. S. Cooper, L. W. Rupp, Jr., B. Batlogg, Y. L. Soo, Z. H. Ming, A. Krol, and Y. H. Kao, Phys. Rev. Lett. **66**, 104 (1991).

[30] M. Taguchi, A. Chainani, K. Horiba, Y. Takata, M. Yabashi, K. Tamasaku, Y. Nishino, D. Miwa, T. Ishikawa, T. Takeuchi, K. Yamamoto, M. Matsunami, S. Shin, T. Yokoya, E. Ikenaga, K. Kobayashi, T. Mochiku, K. Hirata, J. Hori, K. Ishii, F. Nakamura, and T. Suzuki, Phys. Rev. Lett. **95**, 177002 (2005).

[31] Hyeong-Do Kim, Han-Jin Noh, K. H. Kim, and S.-J. Oh, Phys. Rev. Lett. **93**, 126404 (2004).

[32] M. van Veenendaal, Phys. Rev. B **74**, 085118 (2006).

[33] *Proceedings of the Workshop on Hard X-ray Photoelectron Spectroscopy*, edited by J. Zegenhagen and C. Kunz (Elsevier, Amsterdam, 2005) [Nucl. Instrum. Methods: Phys. Res. A **547**, 1 (2005)].

[34] C. J. Powell and A. Jablonski, *NIST Electron Inelastic-Mean-Free-Path Database*, Version 1.2 (National Institute of Standards and Technology, Gaithersburg, MD, 2010).

[35] Y. Takata, M. Yabashi, K. Tamasaku, Y. Nishino, D. Miwa, T. Ishikawa, E. Ikenaga, K. Horiba, S. Shin, M. Arita, K. Shimada, H. Namatame, M. Taniguchi, H. Nohira, T. Hattori, S. Sodergren, B. Wannberg, and K. Kobayashi, Nucl. Instrum. Methods: Phys. Res. A **547**, 50 (2005); T. Ishikawa, K. Tamasaku, and M. Yabashi, *ibid.* **547**, 42 (2005).

[36] A. Y. Gray, C. Papp, S. Ueda, B. Balke, Y. Yamashita, L. Plucinski, J. Minar, J. Braun, E. R. Ylvisaker, C. M. Schneider, W. Pickett, H. Ebert, K. Kobayashi, and C. S. Fadley, Nat. Mater. **10**, 759 (2011).

[37] E. Holmstrom, W. Olovsson, I. A. Abrikosov, A. M. N. Niklasson, B. Johansson, M. Gorgoi, O. Karis, S. Svensson, F. Schafers, W. Braun, G. Ohrwall, G. Andersson, M. Marcellini, and W. Eberhardt, Phys. Rev. Lett. **97**, 266106 (2006).

[38] Aron Walsh, Juarez L. F. Da Silva, Su-Huai Wei, C. Körber, A. Klein, L. F. J. Piper, Alex DeMasi, Kevin E. Smith,

G. Panaccione, P. Torelli, D. J. Payne, A. Bourlange, and R. G. Egdell, Phys. Rev. Lett. **100**, 167402 (2008).
[39]M. Sing, G. Berner, K. Goss, A. Muller, A. Ruff, A. Wetscherek, S. Thiel, J. Mannhart, S. A. Pauli, C. W. Schneider, P. R. Willmott, M. Gorgoi, F. Schafers, and R. Claessen, Phys. Rev. Lett. **102**, 176805 (2009).
[40]M. Takizawa, Y. Hotta, T. Susaki, Y. Ishida, H. Wadati, Y. Takata, K. Horiba, M. Matsunami, S. Shin, M. Yabashi, K. Tamasaku, Y. Nishino, T. Ishikawa, A. Fujimori, and H. Y. Hwang, Phys. Rev. Lett. **102**, 236401 (2009).
[41]K. Horiba, M. Taguchi, A. Chainani, Y. Takata, E. Ikenaga, D. Miwa, Y. Nishino, K. Tamasaku, M. Awaji, A. Takeuchi, M. Yabashi, H. Namatame, M. Taniguchi, H. Kumigashira, M. Oshima, M. Lippmaa, M. Kawasaki, H. Koinuma, K. Kobayashi, T. Ishikawa, and S. Shin, Phys. Rev. Lett. **93**, 236401 (2004).
[42]A. P. Ramirez, Annu. Rev. Mater. Sc. **24**, 453 (1994).
[43]J. S. Gardner, M. J. P. Gingras, and J. E. Greedan, Rev. Mod. Phys. **82**, 53 (2010).
[44]M. Yoshida, M. Takigawa, A. Yamamoto, and H. Takagi, J. Phys. Soc. Jpn. **80**, 034705 (2011).
[45]M. Miyazaki, R. Kadono, K. H. Satoh, M. Hiraishi, S. Takeshita, A. Koda, A. Yamamoto, and H. Takagi, Phys. Rev. B **82**, 094413 (2010).
[46]P. Fulde, K. Penc, and N. Shannon, Ann. Phys. (Leipzig) **11**, 892 (2002).
[47]C. Castelnovo, R. Moessner, and S. L. Sondhi, Nature (London) **451**, 42 (2006).
[48]T. Takahashi, F. Maeda, H. Katayama-Yoshida, Y. Okabe, T. Suzuki, A. Fujimori, S. Hosoya, S. Shamoto, and M. Sato, Phys. Rev. B **37**, 9788 (1988).
[49]G. Pacchioni and P. S. Bagus, Phys. Rev. B **50**, 2576 (1994).
[50]N. Harima, A. Fujimori, T. Sugaya, and I. Terasaki, Phys. Rev. B **67**, 172501 (2003).
[51]P. A. Glans, T. Learmonth, K. E. Smith, J. Guo, A. Walsh, G. W. Watson, F. Terzi, and R. G. Egdell, Phys. Rev. B **71**, 235109 (2005).
[52]K. S. Lee, D. K. Seo, and M. H. Whangbo, J. Solid State Chem. **131**, 405 (1997).
[53]M. Field, B. J. Kennedy, and B. A. Hunter, J. Solid. State Chem. **151**, 25 (2000).
[54]D. A. Shirley, Chem. Phys. Lett. **16**, 220 (1972).
[55]S. Larsson, Chem. Phys. Lett. **40**, 362 (1976).
[56]E. Sokolowski, C. Nordling, and K. Siegbahn, Phys. Rev. **110**, 776 (1958).
[57]J. F. Moulder, W. F. Stickle, P. E. Sobol, and K. D. Bomben, *Handbook of X-ray Photoelectron Spectroscopy* (Physical Electronics, Eden Prairie, MN, 1995).
[58]O. Gunnarsson and K. Schonhammer, Phys. Rev. Lett. **50**, 604 (1983); Phys. Rev. B **28**, 4315 (1983).
[59]G. van der Laan, C. Westra, C. Haas, and G. A. Sawatzky, Phys. Rev. B **23**, 4369 (1981).
[60]F. de Groot and A. Kotani, *Core Level Spectroscopy of Solids, Advances in Condensed Matter Science*, Vol. 6, edited by D. D. Sarma, G. Kotliar, and Y. Tokura (CRC Press, Boca Raton, 2008).
[61]K. Raghavachari and G. W. Trucks, J. Chem. Phys. **91**, 2457 (1989).
[62]P. Mahadevan, N. Shanthi, and D. D. Sarma, Phys. Rev. B **54**, 11199 (1996).
[63]R. D. Shannon, Acta Crystallogr., Sect. A **32**, 751 (1976).
[64]K. B. Helean, S. V. Ushakov, C. E. Brown, A. Navrotsky, J. Lian, R. C. Ewing, J. M. Farmer, and L. A. Boatner, J. Solid. State Chem. **177**, 1858 (2004).
[65]S. Baidya, S. Sarkar, T. Saha-Dasgupta, and D. D. Sarma, Phys. Rev. B **86**, 125117 (2012).
[66]L. Craco, M. S. Laad, S. Leoni, and H. Rosner, Phys. Rev. B **79**, 075125 (2009).
[67]J. S. Lee, Y. S. Lee, K. W. Kim, T. W. Noh, J. Yu, T. Takeda, and R. Kanno, Phys. Rev. B **64**, 165108 (2001).
[68]M. Taguchi, A. Chainani, M. Matsunami, R. Eguchi, Y. Takata, M. Yabashi, K. Tamasaku, Y. Nishino, T. Ishikawa, S. Tsuda, S. Watanabe, C.-T. Chen, Y. Senba, H. Ohashi, K. Fujiwara, Y. Nakamura, H. Takagi, and S. Shin, Phys. Rev. Lett. **104**, 106401 (2010).
[69]R. Eguchi, M. Taguchi, M. Matsunami, K. Horiba, K. Yamamoto, Y. Ishida, A. Chainani, Y. Takata, M. Yabashi, D. Miwa, Y. Nishino, K. Tamasaku, T. Ishikawa, Y. Senba, H. Ohashi, Y. Muraoka, Z. Hiroi, and S. Shin, Phys. Rev. B **78**, 075115 (2008).
[70]P. A. Bhobe, A. Chainani, M. Taguchi, T. Takeuchi, R. Eguchi, M. Matsunami, K. Ishizaka, Y. Takata, M. Oura, Y. Senba, H. Ohashi, Y. Nishino, M. Yabashi, K. Tamasaku, T. Ishikawa, K. Takenaka, H. Takagi, and S. Shin, Phys. Rev. Lett. **104**, 236404 (2010).
[71]Hidekazu Tanaka, Yasutaka Takata, Koji Horiba, Munetaka Taguchi, Ashish Chainani, Shik Shin, Daigo Miwa, Kenji Tamasaku, Yoshinori Nishino, Tetsuya Ishikawa, Eiji Ikenaga, Mitsuhiro Awaji, Akihisa Takeuchi, Tomoji Kawai, and Keisuke Kobayashi, Phys. Rev. B **73**, 094403 (2006).
[72]A. B. Anderson, S. Y. Hong, and J. L. Smialek, J. Phys. Chem. **91**, 4250 (1987).